AGU PUBLICATIONS

Geophysical Research Letters

RESEARCH LETTER
10.1002/2017GL075919

Key Points:
- First observation of intense lion roar emission carried out in Saturn's magnetosheath
- Emission occurs at frequencies of approximately 0.16 f_{ce} as right-hand circularly polarized waves in the spacecraft frame
- Poynting flux directions show that waves are generated at the dawn flank magnetosheath close to the bow shock

Correspondence to:
D. Píša,
dp@ufa.cas.cz

Citation:
Píša, D., Sulaiman, A. H., Santolik, O., Hospodarsky, G. B., Kurth, W. S., & Gurnett, D. A. (2018). First observation of lion roar emission in Saturn's magnetosheath. *Geophysical Research Letters*, *45*, 486–492. https://doi.org/10.1002/2017GL075919

Received 3 OCT 2017
Accepted 23 DEC 2017
Accepted article online 9 JAN 2018
Published online 17 JAN 2018

First Observation of Lion Roar Emission in Saturn's Magnetosheath

D. Píša[1], A. H. Sulaiman[2], O. Santolík[1,3], G. B. Hospodarsky[2], W. S. Kurth[2], and D. A. Gurnett[2]

[1]Institute of Atmospheric Physics CAS, Prague, Czech Republic, [2]Department of Physics and Astronomy, University of Iowa, Iowa City, IA, USA, [3]Faculty of Mathematics and Physics, Charles University in Prague, Prague, Czech Republic

Abstract We present an observation of intense emissions in Saturn's magnetosheath as detected by the Cassini spacecraft. The emissions are observed in the dawn sector (magnetic local time ~06:45) of the magnetosheath over a time period of 11 h before the spacecraft crossed the bow shock and entered the unshocked solar wind. They are found to be narrow-banded with a peak frequency of about 0.16 f_{ce}, where f_{ce} is the local electron gyrofrequency. Using plane wave propagation analysis, we show that the waves are right hand circularly polarized in the spacecraft frame and propagate at small wave normal angles (<10°) with respect to the ambient magnetic field. Electromagnetic waves with the same properties known as "lion roars" have been reported by numerous missions in the terrestrial magnetosheath. Here we show the first evidence such emission outside the terrestrial environment. Our observations suggest that lion roars are a solar-system-wide phenomenon and capable of existing in a broad range of parameter space. This also includes 1 order of magnitude difference in frequencies. We anticipate our result to provide new insight into such emissions in a new parameter regime characterized by a higher plasma beta (owing to the substantially higher Mach number bow shock) compared to Earth.

1. Introduction

A magnetosheath is an intermediate region ahead of a planetary magnetosphere where the solar wind slows down from supersonic to subsonic speeds across a bow shock. Here the interplanetary magnetic field (IMF) carried by the solar wind plasma is compressed and perpendicular electron temperature increases. The electron temperature anisotropy can lead to a growth of intense electromagnetic waves (e.g., Kennel & Petschek, 1966).

Electromagnetic emissions at frequencies 0.1 – 0.5 f_{ce} (~100 Hz), where f_{ce} is the local electron gyrofrequency, known as "lion roars" were first reported in the terrestrial magnetosheath by the OGO-5 satellite (e.g., Smith et al., 1969). Smith and Tsurutani (1976) subsequently discovered that the lion roars are right-hand circularly polarized waves propagating at small wave normal angles (<15°) to the ambient magnetic field, that is, in the whistler mode. Using the Equator-S measurements, Baumjohann et al. (1999) showed narrow-banded waves (0.05 – 0.15f_{ce}) with wave normals almost field-aligned (~0.2°). More oblique (~40° or 150°) waves with a broader frequency band (up to 0.75 f_{ce}) were found in measurements done by Cluster (Maksimovic et al., 2001) and Double Star (Yearby et al., 2005). More recently, Dubinin et al. (2007) showed observations of lion roar emissions at a frequency range 0.1 – 0.2 f_{ce} in the terrestrial magnetosphere.

The lion roars are often observed simultaneously with magnetic dips (Smith & Tsurutani, 1976). These magnetic dips were later identified as mirror-mode waves (Tsurutani et al., 1982) whereby the magnetic field strength is anticorrelated with the electron density. Trapped electrons within the magnetic cavity in the high-β, low magnetic field region can generate waves via the cyclotron resonance instability (Thorne & Tsurutani, 1981). Smith and Tsurutani (1976) proposed an alternative generation mechanism based on a cyclotron overstability caused by field-aligned proton beams with energy of about 10 keV. Using Geotail measurements, Zhang et al. (1998) observed 30% of lion roar bursts with mirror-mode structures and 70% without. The evidence for a source region disassociated with the mirror mode was already suggested by Tsurutani et al. (1982). They concluded that a source region may be located in the flank of the magnetosheath as well. In the flank region, the resonant energy can be as low as the electron thermal energy. Whistler waves grow as the number of resonant electrons increases. The observations of lion roars outside of the mirror-mode

structure were presented, for example, by Zhang et al. (1998) (Type B) and Masood et al. (2006). Another source mechanism was proposed by Dubinin et al. (2007) where they suggested that the observed coherent structure of lion roars in the magnetosphere can be associated with nonlinear properties of Gendrin's whistler waves. A nonlinear system consisting of the electrons and protons can resonate at a frequency where the phase and group speed of the waves are equal. This interaction can lead to the periodic momentum exchange between electrons and protons, giving arise to wave packets.

Lion roars are the most intense whistler-mode emission observed in Earth's magnetosheath, with typical amplitudes of several hundred of pT (e.g., Zhang et al., 1998), peak amplitudes of 0.5 nT inside the magnetic cavities of mirror-mode waves (Baumjohann et al., 2000), and amplitudes as high as 1 nT detected by the Double Star spacecraft (Yearby et al., 2005).

The solar wind conditions at Saturn result in a magnetosheath that has different properties compared to Earth. The typical Parker spiral angle at Saturn's distance (10 AU) is ~90° (see Figure 2 in Píša et al., 2016). The IMF configuration together with the solar wind plasma properties forms a high Alfvénic Mach number (10–100) quasi-perpendicular shock (Sulaiman et al., 2015, 2016). Plasma conditions in Saturn's magnetosheath are variable and reflect fluctuations in the solar wind parameters. The first systematic study of magnetosheath plasma properties at Saturn was presented by Sergis et al. (2013). Based on Cassini's observations, they found that the plasma pressure varies between 6 and 30 pPa, the plasma density between 0.05 and 0.25 cm^{-3}, the plasma temperature between 210 and 370 eV, and plasma flow speed between 170 and 240 $km \cdot s^{-1}$. In the dawn region of Saturn's magnetosphere the average direction of plasma flow projected onto the ecliptic plane and measured counterclockwise from the sunward direction has an angle in the range of 175°–205°. Sergis et al. (2013) also reported the presence of water group ions (W+) with magnetospheric origin in magnetosheath which can locally increase the total plasma pressure. The magnitude of the magnetic field is typically 0.6–1.6 nT and results in a magnetic pressure of 0.2–1.1 pPa. The plasma β is in the range of 10–100. Sergis et al. (2013) concluded that the magnetosheath width does not appear to be very sensitive to the upstream solar wind conditions.

In this paper, we present observations of a lion roar emission event at Saturn obtained by the Cassini spacecraft on 3 July 2005. Further, a part of the time interval with the most intense emission was used for a more detailed wave propagation analysis.

2. Data

The waveform receiver (WFR), a part of the Radio and Plasma Wave Science (RPWS) instrument (Gurnett et al., 2004), collects simultaneous waveforms from up to five sensors in a frequency range of either 1–26 Hz (lower band) or 3 Hz–2.5 kHz (upper band). For the purpose of this study, only the lower band is required. The waveforms are sampled at a frequency of 100 Hz with 12 bit resolution. The WFR snapshot with a length of 20.48 s is available every ~24 s. During the analyzed time period the WFR receiver was operating in a mode in which Channel 1 gathers the electric dipole antenna (E_x) signal, Channel 2 the electric monopole antenna (E_w) signal, and Channels 3–5 collect the B_x, B_y, and B_z search coil signals, respectively. An ambient magnetic field was obtained from the triaxial fluxgate magnetometer which is a part of the magnetometer (MAG) instrument (Dougherty et al., 2004). MAG data with 1 min averages are used to remove high-frequency perturbations and improve the magnetic field direction.

The WFR waveforms measured in the spacecraft coordinate system were transformed into the local field-aligned coordinates (LFAC). The LFAC system is defined as follows: $\hat{z} = \vec{B_0}$, where $\vec{B_0}$ is the direction of the ambient magnetic field as measured by the fluxgate magnetometer, $\hat{y} = \hat{z} \times \vec{X}_{KSO}$, where $\vec{X}_{KSO}$ points from Saturn to the Sun, and $\hat{x}$ completes the orthogonal right-handed system. Consequently, the 5×5 Hermitian cross-spectral matrices (three magnetic and two electric signals) with 64 frequency bins distributed over the frequency range of 1–50 Hz and a time step of 24 s were calculated.

3. Observations

Cassini crossed the magnetopause at ~03:30 UTC on 1 July 2005 and entered the dawn sector (magnetic local time, MLT, ~06:45) of the magnetosheath. The spacecraft experienced multiple bow shock crossings and returned to the Saturnian magnetosphere at ~21:30 UTC on 12 July 2005. A part of Cassini's orbit between 1 and 6 July 2005 projected onto the ecliptic plane is shown in Figure 1a. The gray solid lines represent the

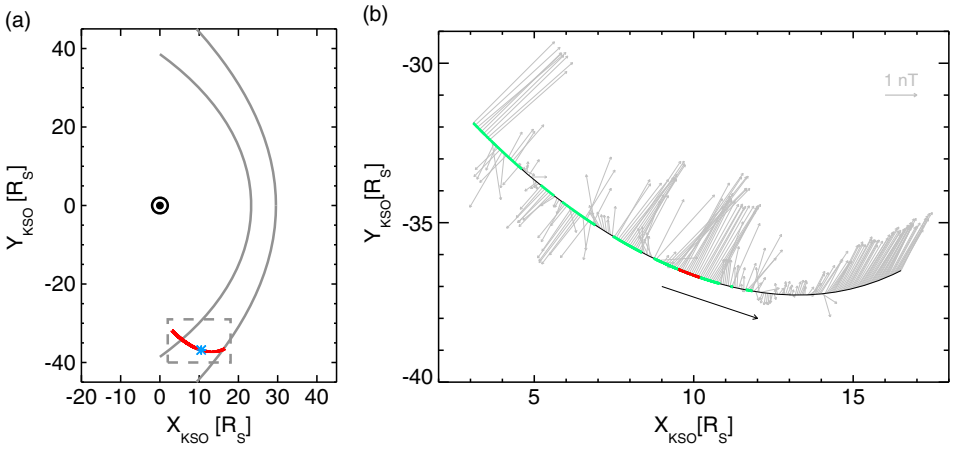

Figure 1. (a) Cassini's orbit between 1 and 6 July 2005 projected onto the ecliptic plane. The solid gray lines show the magnetopause (inner curve), and the bow shock (outer curve), based on models of Arridge et al. (2006) and Went et al. (2011), respectively. The location of both boundaries is calculated for a solar wind dynamic pressure of 26 pPa. The dashed gray rectangle depicts an area shown in Figure 1b. (b) Cassini's positions within the magnetosheath are shown by the green color. The time interval with an intense whistler-mode emission observed on 3 July is plotted in red. The gray arrows represent the magnetic field line projected onto the ecliptic plane measured by the fluxgate magnetometer at 30 min time steps. The black arrow shows the direction of satellite's trajectory.

magnetopause and bow shock positions based on models of Arridge et al. (2006) and Went et al. (2011), respectively, for the solar wind dynamic pressure of 26 pPa. Figure 1b demonstrates the trajectory in more details and illustrates strong variation of plasma conditions inside a flank of the magnetosheath during the analyzed time period. Cassini's positions within the magnetosheath are shown by the green color. The red color represents a time interval (~04:00–14:30 UTC) with intense whistler-mode emissions observed on 3 July 2005. The gray arrows depict the magnetic field direction and intensity projected onto the ecliptic plane measured by the fluxgate magnetometer at 30 min time steps. The black arrow indicates the direction of Cassini's trajectory.

For a detailed wave propagation analysis, the time interval between 03:00 and 09:00 was selected. This time interval covers the most intense emissions and the lower level of instrumental noise, especially in the magnetic components. A similar propagation analysis as was previously done by Santolík et al. (2011) is presented in Figure 2. Figures 2a and 2b show time-frequency spectrograms for the sum of two electric and three magnetic components, respectively. The white solid line represents one half of the electron gyrofrequency calculated from the fluxgate magnetometer measurements. Intense horizontal lines at frequencies 8, 16, and 24 Hz in Figure 2b are instrumental interference with the bus interface unit. Wave propagation properties are only calculated for electric wave intensities higher than 10^{-4}mV^{2}m^{-2}Hz^{-1} and magnetic wave intensities higher than 10^{-5}nT^{2}Hz^{-1}. Coherence in the polarization plane using the singular value decomposition (SVD) of the magnetic spectral matrices (Santolík & Gurnett, 2002) is presented in Figure 2c. The ellipticity of the wave polarization with its sense (Santolík et al., 2002) is shown in Figure 2d, +1 is a right-hand circularly polarized wave and −1 is left-hand circularly polarized. The wave normal angle with respect to the ambient magnetic field obtained from the SVD method of the magnetic spectral matrices (Santolík et al., 2003) is plotted in Figure 2e, 0° for waves propagating parallel with the field and 90° for transverse wave propagation. Figure 2f presents the component of the Poynting flux in the direction of the ambient magnetic field with a level of confidence (Santolík et al., 2001); positive values indicate the parallel propagation and negative values the antiparallel propagation.

The propagation properties shown in Figure 2 are summarized in Figure 3. At each time step, a frequency, F_{max}, with the maximum wave intensity in the sum of electric components for the frequency range of 5–35 Hz was identified. The electric component and frequency range were restricted for times with lower instrumental noise levels and typical frequency band for the intense emissions. All analyzed parameters were averaged for $F_{max}\pm1.5$ Hz. Distribution of normalized peak frequencies is plotted in Figure 3a. Figure 3b shows a distribution of an ellipticity of wave polarization with the polarization sense. A distribution of normal wave angles

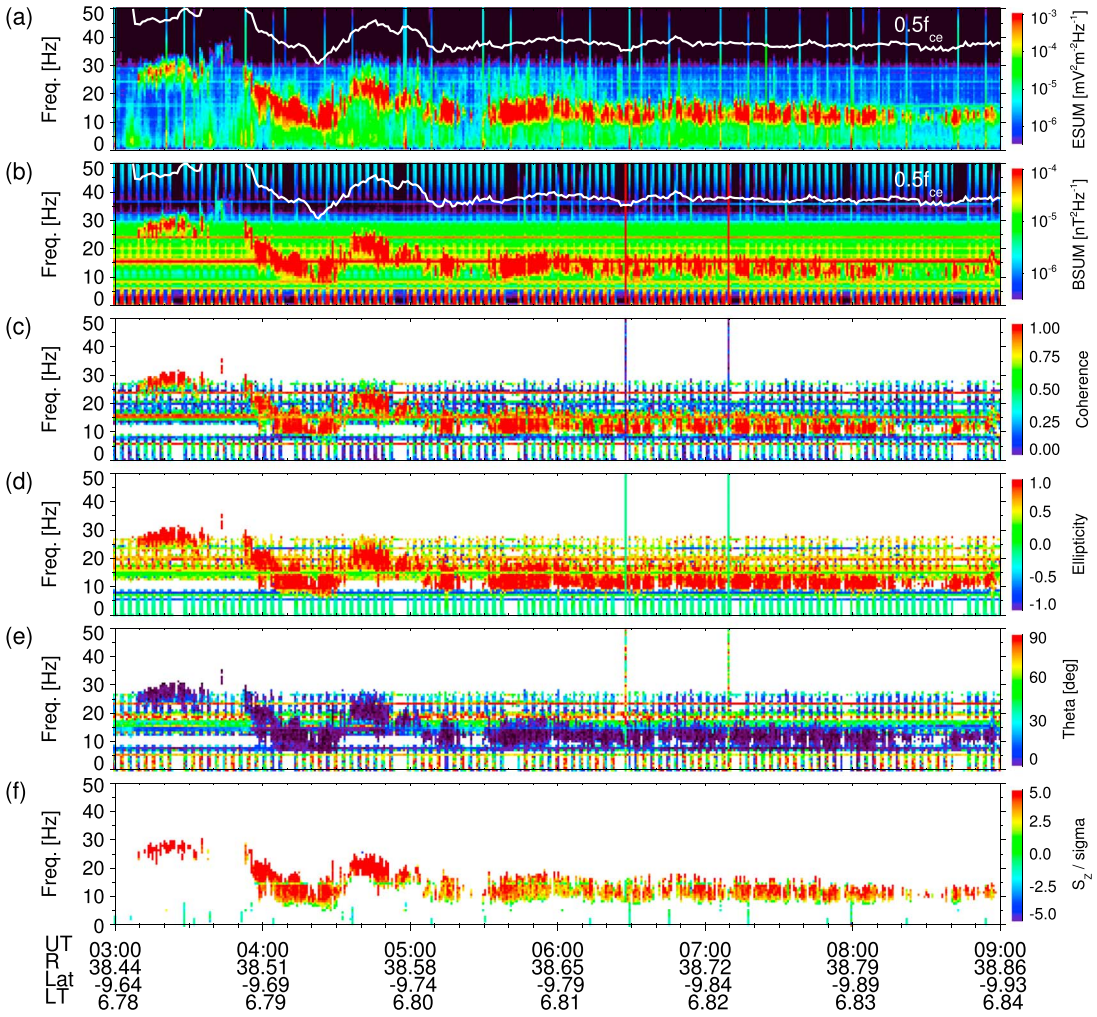

Figure 2. Cassini RPWS/WFR lower band data measured on 3 July 2005. (a and b) Sum of the power spectral densities of two components of electric field and three components of magnetic field, respectively, according to the color bars on the right-hand side, in the frequency range up to 50 Hz. The white line shows one half of the electron gyrofrequency, f_{ce}, calculated from 1 min fluxgate measurements. (c) Coherence in the polarization plane using the SVD method of the magnetic spectral matrices. (d) Ellipticity of the wave polarization combined with the sense of polarization, +1 for right-hand and −1 for the left-hand circularly polarized waves. (e) Polar angle of a wave vector, 0° for waves propagating parallel to the ambient magnetic field and 90° for transverse wave propagation. (f) Component of the Poynting flux along the ambient magnetic field with the level of confidence, positive values indicate parallel propagation and negative values antiparallel propagation.

is presented in Figure 3c. The normalized Poynting flux along the magnetic field line is plotted in Figure 3d. Figure 3e shows a part of the RPWS/WFR waveform snapshot with the whistler-mode wave packets.

4. Discussion and Summary

Cassini measured intense emissions in the dawn sector (MLT∼06:45) of the magnetosheath for more than 11 h before the bow shock crossing and entering the solar wind (∼15:00 UTC). As can be seen in Figures 2a and 2b the emissions are narrow-banded with a relative frequency of ∼0.16 f_{ce} (Figure 3a). The typical magnetic field strength in magnetosheath is around 0.9 nT (Sergis et al., 2013), which yields an electron cyclotron frequency of ∼25 Hz. Under these conditions the lion roar emissions are expected to be observed at a frequency of about 4 Hz (0.16f_{ce}). However, this peak frequency of 4 Hz is very close to receiver lower-frequency cutoff. Therefore, lion roars can be clearly observed from the RPWS/WFR measurements only during time periods with stronger magnetic fields. During the analyzed time period the median magnetic field strength was ∼3 nT resulting to a wave frequency of about 13 Hz (0.16f_{ce}).

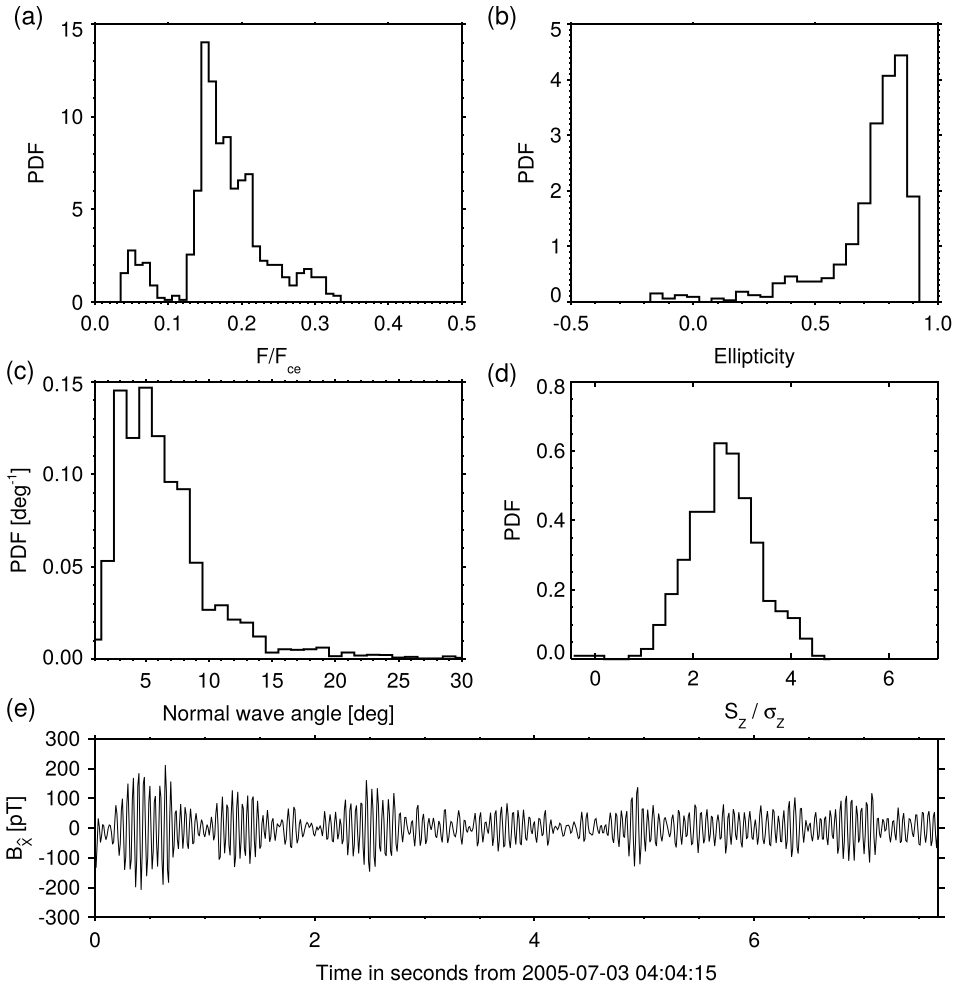

Figure 3. (a) Distribution of normalized frequencies for the most intense spectral peak of the sum of two electric components in Figure 2a. (b) Distribution of the ellipticity of wave polarization with the polarization sense. (c) Distribution of normal wave angles obtained from Figure 2d. (d) Distribution of the normalized Poynting flux component along the magnetic field. (e) An example of the $B_{\hat{x}}$ component of the RPWS/WFR waveform snapshot showing whistler-mode wave packets.

Using the plane wave analysis, it is shown that waves are right hand circularly polarized in the spacecraft frame (Figure 3b) and propagate nearly parallel to the ambient magnetic field ($\theta_{kb}<10°$) as can be seen in Figure 3c. We do not have information about the solar wind speed and direction with respect to the magnetic field; however, we can estimate the maximum Doppler shift. If we assume that the plasma flow is parallel to the ambient magnetic field with a speed of 240 km $\cdot$ s^{-1} (Sergis et al., 2013), the wave frequency of 15 Hz, and a typical refractive index of 100 (estimated from measured data and the method shown in Santolík et al., 2003) the Doppler shift is ~1.2 Hz. Thus, the Doppler shift does not significantly change the wave properties measured in the spacecraft frame.

Although mirror-mode structures were already observed in Saturn's magnetosheath (Cattaneo et al., 1998; Tsurutani et al., 1982), we observed no correlation of wave intensity with the ambient magnetic field fluctuations in contrast with Tsurutani et al. (1982) and Baumjohann et al. (1999), who showed a significant correlation between the occurrence of lion roars and the magnetosheath mirror-mode waves. Zhang et al. (1998) presented significant difference in wave normal directions for events with/without the simultaneous mirror-mode structure. Their events associated with the mirror modes (Type A) propagate almost parallel to the ambient magnetic field ($\theta_{kb}<10°$). Whereas, the events not associated with mirror modes (Type B) have highly oblique wave normal angles (θ_{kb} up to 87°). The higher wave normal angles might be explained by a

remote source region and scattering of the wave vector during a wave propagation to the satellite position (e.g., Masood et al., 2006).

The lack of plasma measurements during this event limits us to determine the local plasma distribution function related to a possible wave source. At Earth Thorne and Tsurutani (1981) showed that waves can be generated by the electron cyclotron instability resulting from the presence of an electron temperature anisotropy ($T_\perp/T_\parallel > 1$). Evidence of lion roars generated via the electron cyclotron instability can often be observed during mirror modes, when conditions for the wave growth are satisfied (Dubinin et al., 2007; Treumann et al., 2000). However, we do not see any connection with the mirror-mode structures during the analyzed event. Small wave normal angles (Figure 3c) and Poynting flux directions (Figure 3d) indicate that waves propagate parallel to the ambient magnetic field lines. Assuming the typical azimuthal angle of the bulk plasma flow in the dawn magnetosheath (175° – 205°, Sergis et al., 2013) and orientation of the magnetic field line (∼60°) shown in Figure 1b (the red part of satellite's orbit), one can see that waves propagate from the flank region of magnetosheath nearly opposite to the plasma flow. Variations of the wave peak frequency (Figures 2a and 2b) follow changes of the local cyclotron frequency. Thus, we deduce that our observations are very close to the probable source region. The existence of the source region at the flank region of magnetosheath is in agreement with Tsurutani et al. (1982) who discussed conditions for wave growth occurring independently of the mirror-mode structures. Typical conditions in Saturn's magnetosheath as observed by Sergis et al. (2013) result in the high plasma-β regime (10 – 100). Under these plasma conditions the characteristic resonant particle energy can be as low as ∼20 eV. During the analyzed event the median magnetic field strength was almost 3 nT. For such strong magnetic field and electron density of ∼0.12 cm^{-3} (obtained from the RPWS Ne proxy data) the characteristic scaling energy is about 180 eV. Then, the resonant energy for electrons is about 670 eV (for f/f_{ce} ∼0.16). An alternative source mechanism involving proton beams (Smith & Tsurutani, 1976) could be satisfied with a streaming energy of about 44 keV (for the critical energy $E_c \simeq 180$ eV and $f/f_{ce} = 0.16$). However, this energy exceeds the magnetosheath streaming energy of ∼0.5 keV and the proton thermal energy of 370 eV (Sergis et al., 2013).

The lion roar emissions observed in Saturn's magnetosheath form coherent whistler-mode wave packet (see in Figure 2c) with amplitudes of a few hundred pT (Figure 3e). Although one can find even stronger amplitudes (>1 nT) inside the terrestrial magnetosheath (Baumjohann et al., 1999; Yearby et al., 2005), these amplitudes are comparable to those of lion roars at Earth (Smith et al., 1969; Zhang et al., 1998).

Intense electromagnetic lion roars have been observed by many missions in the terrestrial magnetosheath (e.g., Smith et al., 1969; Zhang et al., 1998). Here we present the first conclusive evidence of intense lion roar emissions in Saturn's magnetosheath. Emissions are narrow-banded with a peak frequency of about 16% of the local electron gyrofrequency. Waves propagate at small wave normal angles (<10°) with respect to the ambient magnetic field and they are right hand circularly polarized. Our observations of lion roars outside the terrestrial environment suggest that they are a solar-system-wide phenomenon and capable of existing in a board range of parameters including 1 order of magnitude difference in frequencies at Saturn. Future work on identifying the location of dominant sources of the lion roars and plasma conditions favorable for their detection will improve our understanding of the processes at work in unique parameter plasma regimes of outer planets.

Acknowledgments
The authors are grateful to the CASSINI/MAG team for their support and for access to magnetometer data. Observations of the electric and magnetic field experiment RPWS/WFR, RPWS Ne proxy, and the magnetic field instrument MAG on Cassini are available on http://ppi.pds.nasa.gov. This work has been supported by NASA through contract 1415150 with the Jet Propulsion Laboratory, from grants 16-16050Y and 17-08772S of Czech Science Foundation, from the MSMT grant LTAUSA17070, and from the Praemium Academiae award.

References

Arridge, C. S., Achilleos, N., Dougherty, M. K., Khurana, K. K., & Russell, C. T. (2006). Modeling the size and shape of Saturn's magnetopause with variable dynamic pressure. *Journal of Geophysical Research*, *111*, A11227. https://doi.org/10.1029/2005JA011574

Baumjohann, W., Georgescu, E., Fornacon, K.-H., Auster, H. U., Treumann, R. A., & Haerendel, G. (2000). Magnetospheric lion roars. *Annales Geophysicae*, *18*, 406 – 410. https://doi.org/10.1007/s00585-000-0406-2

Baumjohann, W., Treumann, R. A., Georgescu, E., Haerendel, G., Fornacon, K.-H., & Auster, U. (1999). Waveform and packet structure of lion roars. *Annales Geophysicae*, *17*, 1528 – 1534. https://doi.org/10.1007/s00585-999-1528-9

Cattaneo, M. B. B., Basile, C., Moreno, G., & Richardson, J. D. (1998). Evolution of mirror structures in the magnetosheath of Saturn from the bow shock to the magnetopause. *Journal of Geophysical Research: Space Physics*, *103*(A6), 11,961 – 11,972. https://doi.org/10.1029/97JA03683

Dougherty, M. K., Kellock, S., Southwood, D. J., Balogh, A., Smith, E. J., Tsurutani, B. T., … Cowley, S. W. H. (2004). The Cassini magnetic field investigation. *Space Science Reviews*, *114*, 331 – 383. https://doi.org/10.1007/s11214-004-1432-2

Dubinin, E. M., Maksimovic, M., Cornilleau-Wehrlin, N., Fontaine, D., Travnicek, P., Mangeney, A., … Andre, M. (2007). Coherent whistler emissions in the magnetosphere — Cluster observations. *Annales Geophysicae*, *25*, 303 – 315. https://doi.org/10.5194/angeo-25-303-2007

Gurnett, D., Kurth, W., Kirchner, D., Hospodarsky, G., Averkamp, T., Zarka, P., … Pedersen, A. (2004). The Cassini radio and plasma wave investigation. *Space Science Reviews*, *114*(1-4), 395 – 463. https://doi.org/10.1007/s11214-004-1434-0

Kennel, C. F., & Petschek, H. E. (1966). Limit on stably trapped particle fluxes. *Journal of Geophysical Research*, *71*, 1. https://doi.org/10.1029/JZ071i001p00001

Maksimovic, M., Harvey, C. C., Santolík, O., Lacombe, C., de Conchy, Y., Hubert, D., … Balogh, A. (2001). Polarisation and propagation of lion roars in the dusk side magnetosheath. *Annales Geophysicae*, *19*, 1429–1438. https://doi.org/10.5194/angeo-19-1429-2001

Masood, W., Schwartz, S. J., Maksimovic, M., & Fazakerley, A. N. (2006). Electron velocity distribution and lion roars in the magnetosheath. *Annales Geophysicae*, *24*, 1725–1735. https://doi.org/10.5194/angeo-24-1725-2006

Píša, D., O. Santolík, Hospodarsky, G. B., Kurth, W. S., Gurnett, D. A., & Souček, J. (2016). Spatial distribution of Langmuir waves observed upstream of Saturn's bow shock by Cassini. *Journal of Geophysical Research: Space Physics*, *121*, 7771–7784. https://doi.org/10.1002/2016JA022912

Santolík, O., & Gurnett, D. A. (2002). Propagation of auroral hiss at high altitudes. *Geophysical Research Letters*, *29*, 119-1–119-4. https://doi.org/10.1029/2001GL013666

Santolík, O., Gurnett, D. A., Jones, G. H., Schippers, P., Crary, F. J., Leisner, J. S., … Dougherty, M. K. (2011). Intense plasma wave emissions associated with Saturn's moon Rhea,. *Geophysical Research Letters*, *38*, L19204. https://doi.org/10.1029/2011GL049219

Santolík, O., Lefeuvre, F., Parrot, M., & Rauch, J. L. (2001). Complete wave-vector directions of electromagnetic emissions: Application to INTERBALL-2 measurements in the nightside auroral zone. *Journal of Geophysical Research*, *106*, 13,191–13,202. https://doi.org/10.1029/2000JA000275

Santolík, O., Parrot, M., & Lefeuvre, F. (2003). Singular value decomposition methods for wave propagation analysis. *Radio Science*, *38*, 1010. https://doi.org/10.1029/2000RS002523

Santolík, O., Pickett, J. S., Gurnett, D. A., & Storey, L. R. O. (2002). Magnetic component of narrowband ion cyclotron waves in the auroral zone. *Journal of Geophysical Research*, *107*, 1444. https://doi.org/10.1029/2001JA000146

Sergis, N., Jackman, C. M., Masters, A., Krimigis, S. M., Thomsen, M. F., Hamilton, D. C., … Coates, A. J. (2013). Particle and magnetic field properties of the Saturnian magnetosheath: Presence and upstream escape of hot magnetospheric plasma. *Journal of Geophysical Research: Space Physics*, *118*, 1620–1634. https://doi.org/10.1002/jgra.50164

Smith, E. J., & Tsurutani, B. T. (1976). Magnetosheath lion roars. *Journal of Geophysical Research*, *81*, 2261–2266. https://doi.org/10.1029/JA081i013p02261

Smith, E. J., Holzer, R. E., & Russell, C. T. (1969). Magnetic emissions in the magnetosheath at frequencies near 100 Hz. *Journal of Geophysical Research*, *74*, 3027–3036. https://doi.org/10.1029/JA074i011p03027

Sulaiman, A. H., Masters, A., Dougherty, M. K., Burgess, D., Fujimoto, M., & Hospodarsky, G. B. (2015). Quasiperpendicular high Mach number shocks. *Physical Review Letters*, *115*(12), 125001. https://doi.org/10.1103/PhysRevLett.115.125001

Sulaiman, A. H., Masters, A., & Dougherty, M. K. (2016). Characterization of Saturn's bow shock: Magnetic field observations of quasi-perpendicular shocks. *Journal of Geophysical Research: Space Physics*, *121*, 4425–4434. https://doi.org/10.1002/2016JA022449

Thorne, R. M., & Tsurutani, B. T. (1981). The generation mechanism for magnetosheath lion roars. *Nature*, *293*, 384–386. https://doi.org/10.1038/293384a0

Treumann, R. A., Georgescu, E., & Baumjohann, W. (2000). Lion roar trapping in mirror modes. *Geophysical Research Letters*, *27*, 1843–1846. https://doi.org/10.1029/2000GL003767

Tsurutani, B. T., Smith, E. J., Anderson, R. R., Ogilvie, K. W., Scudder, J. D., Baker, D. N., & Bame, S. J. (1982). Lion roars and nonoscillatory drift mirror waves in the magnetosheath. *Journal of Geophysical Research*, *87*, 6060–6072. https://doi.org/10.1029/JA087iA08p06060

Went, D. R., Hospodarsky, G. B., Masters, A., Hansen, K. C., & Dougherty, M. K. (2011). A new semiempirical model of Saturn's bow shock based on propagated solar wind parameters. *Journal of Geophysical Research*, *116*, A07202. https://doi.org/10.1029/2010JA016349

Yearby, K. H., Alleyne, H. S. C. K., Cornilleau-Wehrlin, N., Santolik, O., Balikhin, M. A., Walker, S. N., … Lahiff, A. (2005). Observations of lion roars in the magnetosheath by the STAFF/DWP experiment on the Double Star TC-1 spacecraft. *Annales Geophysicae*, *23*, 2861–2866. https://doi.org/10.5194/angeo-23-2861-2005

Zhang, Y., Matsumoto, H., & Kojima, H. (1998). Lion roars in the magnetosheath: The geotail observations. *Journal of Geophysical Research*, *103*(A3), 4615–4626. https://doi.org/10.1029/97JA02519